ELSEVIER

International Journal of Solids and Structures 41 (2004) 2429–2446

INTERNATIONAL JOURNAL OF SOLIDS and STRUCTURES

www.elsevier.com/locate/ijsolstr

Three-dimensional analysis of cross-ply laminated cylindrical panels with weak interfaces

W.Q. Chen [a,*], Y.F. Wang [b], J.B. Cai [a], G.R. Ye [a]

[a] *Department of Civil Engineering, Zhejiang University, Zheda Road 38, Hangzhou 310027, PR China*
[b] *Hangzhou Radio and TV University, Hangzhou 310012, PR China*

Received 29 June 2003; received in revised form 11 December 2003

Abstract

The bending and free vibration of a simply-supported, cross-ply laminated cylindrical panel with weak interfaces are investigated in this study. The problem is solved using three-dimensional state-space approach coupled with the layer-wise method, which turns the state equation with variable coefficients into one with constant coefficients. The weak interfaces are modeled as spring layers. Their effects on the integrity of the laminate panel are accounted for by integrating the so-called interfacial transfer matrices into the global transfer matrix. The cylindrical bending of the panel is also considered, and an exact static state-space solution is derived. Comprehensive numerical results are presented and some practical issues of importance to engineering applications are discussed.

Keywords: Cross-ply laminate; Cylindrical panel; Weak interface; State-space approach; Spring-layer model

1. Introduction

Problems of composites with weak or imperfect bonding interfaces have been subjected to intense research in the recent decades (Aboudi, 1987; Hashin, 1990, 1991; Chaboche et al., 2001). In the structural level, the interface between two adjacent layers in laminated plates or shells may be weakened or even broken due to external loading or aging of interface bonding. On the other hand, weak interface is occasionally artificially introduced into a laminate to tailor its mechanical properties (Clegg, 1992; Kuo and Kriven, 1996), because it has been found that laminates with weak interfaces have high fracture toughness (Zeng and Jiang, 2001). In general, these weak and damaged interfaces (including delamination and interlayer slip, as limiting cases) degrade the integrity of a laminate structure. For example, they may seriously reduce the rigidity of a laminated panel (Barbero and Reddy, 1991). They may also cause significant shift of natural frequencies from those of a perfectly bonded laminated panel (Cheng et al., 2000). For the purpose of better evaluation or health diagnosis of laminated structures in service, it is highly desirable to

* Corresponding author. Tel.: +86-571-87952284; fax: +86-571-87952165.
E-mail addresses: chenwq@ccea.zju.edu.cn, chenwq@rocketmail.com (W.Q. Chen).

0020-7683/$ - see front matter © 2004 Elsevier Ltd. All rights reserved.
doi:10.1016/j.ijsolstr.2003.12.018

develop analytical methods that can accurately account for effects of weak interfaces in a laminated structure under static or dynamic loadings. Previous work reported in literature has been largely focused on developing or using two-dimensional (2D) laminate plate or shell theories. Barbero and Reddy (1991) suggested a layer-wise laminated plate theory, in which the delaminations of layers were modeled by jump discontinuity conditions at the interfaces. Tenek et al. (1993) investigated the effect of delamination on free vibration of composite plates by the three-dimensional (3D) finite element method (FEM). Point and Sacco (1995) developed a delamination model for composite plates by adopting an adhesion law to simulate the behavior of interface. Barbero et al. (1995) proposed an FEM contact/friction analysis of composite joints, in which an orthotropic Coulomb friction law was employed. Di Sciuva (1997) derived the controlling equations with the consideration of geometric non-linearity for laminated plates with interlaminar slips.

Linear spring-layer model has been widely used to model the load transferring at interfaces between constituent components or adjacent layers (Aboudi, 1987; Hashin, 1990, 1991). In the structural level, Liu et al. (1994) developed a 2D laminate theory for delaminated composite plates. The general linear model of interfaces employed by Liu et al. (1994) actually is identical to the linear spring-layer model mentioned above. The linear interfacial model is very convenient to use, although it is only adequate for modeling the initial response of delaminated structures. A lot of work based on this linear spring-layer model has been reported ever since (Cheng et al., 1996a,b; Williams and Addessio, 1997; Cheng et al., 2000; Librescu and Schmidt, 2001; Soldatos and Shu, 2001; and the references cited therein). The model is summarized in Eq. (1) as below for a laminated cylindrical panel shown in Fig. 1:

$$\begin{aligned} &\sigma_r^{(k+1)} = \sigma_r^{(k)} = [u_r^{(k+1)} - u_r^{(k)}]/R_r^{(k)}, \quad \tau_{r\theta}^{(k+1)} = \tau_{r\theta}^{(k)} = [u_\theta^{(k+1)} - u_\theta^{(k)}]/R_\theta^{(k)}, \\ &\tau_{rz}^{(k+1)} = \tau_{rz}^{(k)} = [u_z^{(k+1)} - u_z^{(k)}]/R_z^{(k)}, \quad \text{at } r = r_k, \end{aligned} \tag{1}$$

where $\sigma_r^{(k)}$, $\tau_{r\theta}^{(k)}$ and $\tau_{rz}^{(k)}$ are stresses in the kth layer, and $R_i^{(k)}$ $(i = r, \theta, z)$ are the compliance constants of the interface between the kth layer and $(k+1)$th layer. It is clear that when $R_i^{(k)} \to 0$, the displacements will be continuous across the interface, implying a perfect bonding, while $R_i^{(k)} \to \infty$ indicates that the kth layer and $(k+1)$th layer are completely separated from each other. If $R_r^{(k)} \to 0$ while $R_\theta^{(k)}$ and $R_z^{(k)}$ have non-zero finite values, an interlaminar shear slip is admitted at the kth interface.

While they are widely used in laminated panel analyses because of their simplicity and cost effectiveness, the applicability and validity of these simplified or reduced-order 2D plate/shell theories must be carefully examined by comparisons either against extensive numerical modeling or 3D exact elasticity solutions. In this sense, simple, analytical 3D elastic solutions are of unique importance because they can be used as

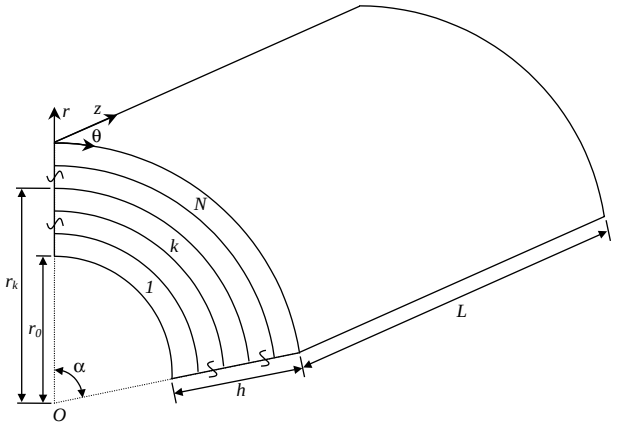

Fig. 1. Geometry of a laminated cylindrical panel and cylindrical coordinates.

simple, inexpensive yard-sticks to appraise any 2D plate/shell theories. There are a lot of exact 3D solutions available in literature but most of them work only for perfectly bonded laminated plates and shells (Pagano, 1969; Srinivas and Rao, 1970; Ren, 1987; Varadan and Bhaskar, 1991; Jing and Tzeng, 1995). Little has been done on laminates with interlaminar bonding imperfections. Williams and Addessio (1997) extended Pagano's solution to a laminated plate in cylindrical bending with delaminations by using linear interfacial constitutive relations (i.e. the spring-layer model). Theoretically all the above-mentioned exact solutions for perfectly bonded laminates can be extended to account for the effects of weak interfaces using the linear spring-layer model. However, conventional 3D elasticity solutions usually suffer from high computational cost when dealing with a laminate made up of a large number of plies (Noor and Burton, 1990).

State-space approach (or initial function method) has been developed for a long time (Vlasov and Leontev, 1966; Bahar, 1975). This method is very effective in analysis of layered elastic systems because (1) the boundary and continuity conditions are directly expressed in terms of state variables, which can be solved from the governing state equation; and (2) the final solving equations remain the same small number no matter how many layers are considered. It has become an important elasticity method in modern structural analysis (Fan and Ye, 1990; Fan and Zhang, 1992a,b; Ye and Soldatos, 1994; Xu and Noor, 1996; Chen and Ding, 2001; Tarn, 2002). Note that even within the simplified theories, the state-space solution also exhibits certain advantage (Khdeir and Reddy, 1997). Chen et al. (2003) recently derived a state-space solution for a simply-supported laminated rectangular plate featuring interlaminar bonding imperfections.

In this paper, we use the state-space approach coupled with the general linear spring-layer model to analyze the 3D bending and free vibration of simply supported, cross-ply laminated cylindrical panels with weak interfaces. Compared to the analysis for perfect laminated cylindrical panels (Fan and Zhang, 1992a), only the interfacial transfer matrices of the spring-layers representing the weak interfaces need to be integrated into the global transfer matrix (Chen et al., 2003). The state equation for laminated cylindrical panel in cylindrical bending is also presented. In particular, an exact state-space solution is given in Appendix B for the static bending problem by using a variable substitution technology. Some numerical examples are considered and results of importance to engineering practices are discussed.

2. State-space formulations

In this section, we give a brief review of the state-space formulations presented in Fan and Zhang (1992a) for the reader's convenience, but with a special non-dimensionalization. Considering an N-layered cross-ply cylindrical panel, as shown in Fig. 1, the constitutive relations are (Whitney, 1987; Jing and Tzeng, 1995)

$$
\begin{aligned}
\sigma_z &= c_{11}\frac{\partial u_z}{\partial z} + c_{12}\left(\frac{1}{r}\frac{\partial u_\theta}{\partial \theta} + \frac{u_r}{r}\right) + c_{13}\frac{\partial u_r}{\partial r},\\
\sigma_\theta &= c_{12}\frac{\partial u_z}{\partial z} + c_{22}\left(\frac{1}{r}\frac{\partial u_\theta}{\partial \theta} + \frac{u_r}{r}\right) + c_{23}\frac{\partial u_r}{\partial r},\\
\sigma_r &= c_{13}\frac{\partial u_z}{\partial z} + c_{23}\left(\frac{1}{r}\frac{\partial u_\theta}{\partial \theta} + \frac{u_r}{r}\right) + c_{33}\frac{\partial u_r}{\partial r},\\
\tau_{r\theta} &= c_{44}\left(\frac{1}{r}\frac{\partial u_r}{\partial \theta} + \frac{\partial u_\theta}{\partial r} - \frac{u_\theta}{r}\right), \quad \tau_{rz} = c_{55}\left(\frac{\partial u_z}{\partial r} + \frac{\partial u_r}{\partial z}\right),\\
\tau_{\theta z} &= c_{66}\left(\frac{\partial u_\theta}{\partial z} + \frac{1}{r}\frac{\partial u_z}{\partial \theta}\right),
\end{aligned}
\tag{2}
$$

where c_{ij} are elastic constants, σ_i and τ_{ij} are normal and shear stress components, respectively. The following state equation can be easily derived from Eq. (2) and the equations of motion (Fan and Zhang, 1992a)

$$\frac{\partial}{\partial r}[u_r, u_\theta, u_z, \sigma_r, \tau_{r\theta}, \tau_{rz}]^{\mathrm{T}} = \mathbf{N}(r)[u_r, u_\theta, u_z, \sigma_r, \tau_{r\theta}, \tau_{rz}]^{\mathrm{T}}, \tag{3}$$

where the matrix $\mathbf{N}(r)$ is given in Appendix A. Note that the derivation of Eq. (3) is fundamental and straightforward, and the reader is referred to any previous paper on state-space approach for a very similar procedure.

An analytical solution can be obtained for the following simply-supported boundary conditions, i.e.

$$\begin{aligned} &\sigma_z = u_\theta = u_r = 0, \quad \text{at } z = 0, L, \\ &\sigma_\theta = u_z = u_r = 0, \quad \text{at } \theta = 0, \alpha. \end{aligned} \tag{4}$$

In fact, we can assume

$$\begin{Bmatrix} u_r \\ u_\theta \\ u_z \\ \sigma_r \\ \tau_{r\theta} \\ \tau_{rz} \end{Bmatrix} = \begin{Bmatrix} r_0\bar{u}_r(\xi)\sin(m\pi\eta)\sin(n\pi\zeta) \\ r_0\bar{u}_\theta(\xi)\cos(m\pi\eta)\sin(n\pi\zeta) \\ r_0\bar{u}_z(\xi)\sin(m\pi\eta)\cos(n\pi\zeta) \\ c_{44}^{(1)}\bar{\sigma}_r(\xi)\sin(m\pi\eta)\sin(n\pi\zeta) \\ c_{44}^{(1)}\bar{\tau}_{r\theta}(\xi)\cos(m\pi\eta)\sin(n\pi\zeta) \\ c_{44}^{(1)}\bar{\tau}_{rz}(\xi)\sin(m\pi\eta)\cos(n\pi\zeta) \end{Bmatrix} \exp(\mathrm{i}\omega t), \tag{5}$$

where $\xi = r/r_0$, $\eta = \theta/\alpha$, and $\zeta = z/L$ are dimensionless coordinates, m and n are the half-wave numbers in the circumferential and axial directions, respectively, $c_{44}^{(1)}$ represents the elastic constant of the first layer (the bottom layer), and ω is the circular frequency. Eq. (5) is the solution to the bending problem if $\omega = 0$; otherwise it is a solution (eigen-mode) for free vibration of the panel. It can be readily shown that Eq. (5) satisfies the simply supported conditions of Eq. (4) automatically. Substituting Eq. (5) into Eq. (3) yields

$$\frac{\mathrm{d}}{\mathrm{d}\xi}\mathbf{V}(\xi) = \mathbf{A}(\xi)\mathbf{V}(\xi), \tag{6}$$

where $\mathbf{V}(\xi) = [\bar{u}_r(\xi), \bar{u}_\theta(\xi), \bar{u}_z(\xi), \bar{\sigma}_r(\xi), \bar{\tau}_{r\theta}(\xi), \bar{\tau}_{rz}(\xi)]^{\mathrm{T}}$, and the non-dimensional coefficient matrix $\mathbf{A}(\xi)$ is also listed in Appendix A. The solution to Eq. (6) is not straightforward because $\mathbf{A}(\xi)$ varies with ξ. Fan and Zhang (1992a,b) suggested a layer-wise method (LWM) to obtain the approximate analytical solution. According to this method, the kth layer in the panel is further equally divided into n_k sub-layers, each with a very small thickness so that $\mathbf{A}(\xi)$ can be taken as a constant. Under this condition, the solution in the lth sub-layer in the kth layer can be obtained per matrix theory (Bellman, 1970) as

$$\mathbf{V}(\xi) = \exp[\mathbf{A}(\xi_{k,l,m})(\xi - \xi_{k,l,0})]\mathbf{V}(\xi_{k,l,0}) \quad (\xi_{k,l,0} \leqslant \xi \leqslant \xi_{k,l,1},\ l = 1, 2, \ldots, n_k;\ k = 1, 2, \ldots, N), \tag{7}$$

where $\xi_{k,l,0}$, $\xi_{k,l,1}$ and $\xi_{k,l,m}$ are the dimensionless radial coordinates at the lower, upper and intermediate surfaces of the lth sub-layer respectively, i.e.

$$\begin{aligned} &\xi_{k,l,0} = (l-1)(\xi_k - \xi_{k-1})/n_k, \quad \xi_{k,l,1} = l(\xi_k - \xi_{k-1})/n_k, \\ &\xi_{k,l,m} = (\xi_{k,l,0} + \xi_{k,l,1})/2, \end{aligned} \tag{8}$$

in which $\xi_0 = 1$, $\xi_k = r_k/r_0 = (r_0 + \sum_{j=1}^{k} h_j)/r_0$, and h_k is the thickness of the kth layer. Setting $\xi = \xi_{k,l,1}$ in Eq. (7) yields

$$\mathbf{V}(\xi_{k,l,1}) = \mathbf{T}_{k,l}\mathbf{V}(\xi_{k,l,0}), \tag{9}$$

where $\mathbf{T}_{k,l} = \exp[\mathbf{A}(\xi_{k,l,m})(\xi_k - \xi_{k-1})/n_k]$ is the transfer matrix of the lth sub-layer in the kth layer. Taking account of the continuity conditions at the fictitious interfaces, i.e.

$$\mathbf{V}(\xi_{k,l+1,0}) = \mathbf{V}(\xi_{k,l,1}) \quad (l = 1, 2, \ldots, n_k - 1), \tag{10}$$

we can easily derive from Eq. (9)

$$\mathbf{V}_1^{(k)} = \mathbf{M}_k \mathbf{V}_0^{(k)}, \tag{11}$$

where $\mathbf{V}_1^{(k)}$ and $\mathbf{V}_0^{(k)}$ are the state vectors at the upper and lower surfaces, respectively, of the kth layer, and $\mathbf{M}_k = \prod_{l=n_k}^{1} \mathbf{T}_{k,l}$ is the transfer matrix of that layer. Similarly, we have for the $(k+1)$th layer

$$\mathbf{V}_1^{(k+1)} = \mathbf{M}_{k+1} \mathbf{V}_0^{(k+1)}. \tag{12}$$

A short discussion is presented here regarding the property of the matrix $\mathbf{A}(\xi)$. As we can see from Eq. (A.4), all elements are functions of ξ^0, ξ^{-1} and ξ^{-2}. For a cylindrical panel considered in this paper, we have $\xi \geqslant 1$, i.e. the matrix $\mathbf{A}(\xi)$ is regular without any singular point. Thus, the variation of matrix $\mathbf{A}(\xi)$ with ξ is rather gentle. This implies that by using the LWM, a relatively small number of sub-layers are necessary to acquire high accurate results. It will be further discussed through numerical example.

3. Imperfect bonding conditions and treatment

The boundary conditions at a weak interface have been given in Eq. (1). It can be re-expressed as follows by applying Eq. (5)

$$\mathbf{V}_0^{(k+1)} = \mathbf{P}_k \mathbf{V}_1^{(k)}, \tag{13}$$

where $\mathbf{P}_k$ can be termed as the interfacial transfer matrix defined as

$$\mathbf{P}_k = \begin{bmatrix} 1 & 0 & 0 & \bar{R}_r^{(k)} & 0 & 0 \\ 0 & 1 & 0 & 0 & \bar{R}_\theta^{(k)} & 0 \\ 0 & 0 & 1 & 0 & 0 & \bar{R}_z^{(k)} \\ 0 & 0 & 0 & 1 & 0 & 0 \\ 0 & 0 & 0 & 0 & 1 & 0 \\ 0 & 0 & 0 & 0 & 0 & 1 \end{bmatrix}. \tag{14}$$

Here $\bar{R}_i^{(k)} = c_{44}^{(1)} R_i^{(k)}/r_0$ $(i = r, \theta, z)$ are dimensionless compliance coefficients of the interfaces. For a perfect interface, $R_i^{(k)} = 0$ and $\mathbf{P}_k = \mathbf{I}$ ($\mathbf{I}$ being the identity matrix).

From Eqs. (11)–(13), a relation between state vectors at the upper surface of the $(k+1)$th layer and the lower surface of the kth layer can be established

$$\mathbf{V}_1^{(k+1)} = \mathbf{M}_{k+1} \mathbf{P}_k \mathbf{M}_k \mathbf{V}_0^{(k)}. \tag{15}$$

Continuing the above procedure, the relation between state vectors at the top and bottom surfaces of the laminated cylindrical panel is finally obtained

$$\mathbf{V}_1^{(N)} = \mathbf{S} \mathbf{V}_0^{(1)}, \tag{16}$$

where $\mathbf{S} = \left(\prod_{j=N}^{2} \mathbf{M}_j \mathbf{P}_{j-1}\right)\mathbf{M}_1$ is the global transfer matrix for a laminated cylindrical panel with weak interfaces. In the case of a perfectly bonded laminate all $\mathbf{P}_j$ become unit. It follows that $\mathbf{S} = \prod_{j=N}^{1} \mathbf{M}_j$, which is the same as that in Fan and Zhang (1992a).

4. Boundary conditions and solutions

4.1. Bending under surface pressure

First, consider the bending problem ($\omega = 0$) of the panel subjected to generally distributed normal loads $p(\theta, z)$ and $q(\theta, z)$ applied on the bottom and top surfaces, respectively. The loads can be expanded in terms of double sine functions as follows:

$$\begin{aligned} p(\theta, z) &= c_{44}^{(1)} \sum_{m=1}^{\infty} \sum_{n=1}^{\infty} a_{mn} \sin(m\pi\eta) \sin(n\pi\zeta), \\ q(\theta, z) &= c_{44}^{(1)} \sum_{m=1}^{\infty} \sum_{n=1}^{\infty} b_{mn} \sin(m\pi\eta) \sin(n\pi\zeta), \end{aligned} \tag{17}$$

where $[a_{mn}, b_{mn}] = [4/c_{44}^{(1)}] \int_0^1 \int_0^1 [p(\eta, \zeta), q(\eta, \zeta)] \sin(m\pi\eta) \sin(n\pi\zeta)\, \mathrm{d}\eta\, \mathrm{d}\zeta$. For an arbitrary couple of (m, n), the surface boundary conditions are

$$\bar{\sigma}_r(\xi_0) = a_{mn}, \quad \bar{\sigma}_r(\xi_N) = b_{mn}, \quad \bar{\tau}_{r\theta}(\xi_0) = \bar{\tau}_{rz}(\xi_0) = \bar{\tau}_{r\theta}(\xi_N) = \bar{\tau}_{rz}(\xi_N) = 0. \tag{18}$$

From Eqs. (16) and (18), we can calculate the unknown state variables at the bottom surface by

$$\begin{bmatrix} S_{41} & S_{42} & S_{43} \\ S_{51} & S_{52} & S_{53} \\ S_{61} & S_{62} & S_{63} \end{bmatrix} \begin{Bmatrix} \bar{u}_r(\xi_0) \\ \bar{u}_\theta(\xi_0) \\ \bar{u}_z(\xi_0) \end{Bmatrix} = \begin{Bmatrix} b_{mn} - S_{44} a_{mn} \\ -S_{54} a_{mn} \\ -S_{64} a_{mn} \end{Bmatrix}, \tag{19}$$

where S_{ij} are elements of the matrix $\mathbf{S}$. The state vector for an arbitrary value of ξ are then determined by

$$\begin{aligned} &\mathbf{V}(\xi) = \mathbf{T}_1(\xi)\mathbf{V}_0^{(1)} \quad (\xi_0 \leqslant \xi \leqslant \xi_1), \\ &\mathbf{V}(\xi) = \mathbf{T}_2(\xi)\mathbf{P}_1\mathbf{M}_1\mathbf{V}_0^{(1)} \quad (\xi_1 \leqslant \xi \leqslant \xi_2), \\ &\mathbf{V}(\xi) = \mathbf{T}_k(\xi)\left(\prod_{j=k-1}^{2} \mathbf{M}_j \mathbf{P}_{j-1}\right)\mathbf{M}_1\mathbf{V}_0^{(1)} \quad (\xi_{k-1} \leqslant \xi \leqslant \xi_k;\ k = 3, 4, \ldots, N). \end{aligned} \tag{20}$$

The three induced variables are then calculated from the state variables by Eq. (A.3).

It is noted here that for a cross-ply laminated cylindrical panel with $L \to \infty$, the cylindrical bending problem arises (Ren, 1987). In this case, we have only two non-zero displacements u_r and u_θ, and both are independent of the coordinate z. The corresponding state equation can be obtained as

$$\frac{\partial}{\partial r}\begin{Bmatrix} u_\theta \\ u_r \\ \tau_{r\theta} \\ \sigma_r \end{Bmatrix} = \begin{bmatrix} \frac{1}{r} & -\frac{1}{r}\frac{\partial}{\partial\theta} & \frac{1}{c_{44}} & 0 \\ -\frac{c_{23}}{c_{33}}\frac{1}{r}\frac{\partial}{\partial\theta} & -\frac{c_{23}}{c_{33}}\frac{1}{r} & 0 & \frac{1}{c_{33}} \\ \rho\frac{\partial^2}{\partial t^2} - \frac{k_3}{r^2}\frac{\partial^2}{\partial\theta^2} & -\frac{k_3}{r^2}\frac{\partial}{\partial\theta} & -\frac{2}{r} & -\frac{c_{23}}{c_{33}}\frac{1}{r}\frac{\partial}{\partial\theta} \\ \frac{k_3}{r^2}\frac{\partial}{\partial\theta} & \rho\frac{\partial^2}{\partial t^2} + \frac{k_3}{r^2} & -\frac{1}{r}\frac{\partial}{\partial\theta} & \left(\frac{c_{23}}{c_{33}} - 1\right)\frac{1}{r} \end{bmatrix} \begin{Bmatrix} u_\theta \\ u_r \\ \tau_{r\theta} \\ \sigma_r \end{Bmatrix}. \tag{21}$$

The proceeding analysis is then similar and omitted here for brevity. However, an exact static solution can be obtained if we rewrite Eq. (21) and employ the variable substitution technique. This is given in Appendix B.

The solution can serve as a yard-stick to examine the convergence behavior of the LWM suggested by Fan and Zhang (1992a,b).

4.2. Free vibration

If the free vibration problem is considered, the right-hand term in Eq. (19) vanishes because of the traction-free conditions. In this case, the following frequency equation is obtained

$$\begin{vmatrix} S_{41} & S_{42} & S_{43} \\ S_{51} & S_{52} & S_{53} \\ S_{61} & S_{62} & S_{63} \end{vmatrix} = 0. \tag{22}$$

After the frequency ω is solved from the above equation, the vibrational modes of displacements at the bottom surface can be determined from the homogeneous equation of Eq. (19).

5. Numerical examples

For clarity, the following rules are applied in the discussion of this section:

(a) The notation system in Whitney (1987) is adopted to denote the layer stacking sequence from the top to bottom. Each layer involved in the N-layer laminated cylindrical panel is considered to have identical thickness (h/N) and density ratio.
(b) The fiber orientation (0° or 90°) is denoted by an angle measured from the z-axis to the fiber direction.
(c) $R_r^{(k)} = 0$ at each interface to avoid the unphysical material penetration (Cheng et al., 1996a,b). It is noted that, under this condition although the radial displacement u_r is continuous across any weak interface, tangential sliding is allowed. Furthermore, we assume that the weakness of any particular interface is uniform and can be expressed as a non-dimensional compliance parameter, $\bar{R}^{(k)} = E_T R_\theta^{(k)}/h = E_T R_z^{(k)}/h$. However, weakness of different interfaces can be different.
(d) The following material constants are employed in all numerical examples:

$$E_L/E_T = 25, \quad G_{LT}/E_T = 0.5, \quad G_{TT}/E_T = 0.2, \quad \mu_{LT} = \mu_{TT} = 0.25, \tag{23}$$

where E is the Young's modulus, G the shear modulus, μ the Poisson's ratio and subscripts L and T indicate, respectively, directions parallel and perpendicular to the fibers. The transformation from the above engineering constants to the elastic stiffness constants c_{ij} can be found in Jones (1975).

To check the correctness of the program written by Mathematica, the numerical examples in Fan and Zhang (1992a) for perfectly bonded, laminated cylindrical panel are revisited and identical results are obtained. In Fan and Zhang (1992a), the convergence behavior of the LWM was studied through comparison of results for different sub-layer numbers. Here an example is further given by considering the cylindrical bending of a perfect cylindrical panel, of which the exact elasticity solution is available (Ren, 1987). An exact solution based on 3D state-space formulation is also given in Appendix B. A normal sinusoidal load $q = q_0 \sin(\pi\eta)$ is assumed to act on the top surface. Comparison is listed in Table 1, where the non-dimensional quantities are defined as

$$S = \frac{r_m}{h}, \quad w = \frac{10E_T}{q_0 h S^4} u_r, \quad \sigma_1 = \frac{1}{q_0 S^2}\sigma_z, \quad \sigma_2 = \frac{1}{q_0 S^2}\sigma_\theta, \quad \sigma_3 = \frac{1}{q_0 S}\tau_{r\theta}, \tag{24}$$

with $r_m = (r_N + r_0)/2$ being the mean radius of the panel. It can be seen that the exact state-space solution agrees well with Ren's solution (1987) and the LWM has an excellent convergence characteristic. In fact, the

Table 1
Verification of LWM: A three-ply ([90/0/90°]) perfect cylindrical panel in cylindrical bending subjected to sinusoidal load $q = q_0 \sin(\pi\eta)$ at the top surface ($\alpha = \pi/3$)

Quantity	S	Ren (1987)	State-space approach			
			Exact	LWM, 30[a]	LWM, 20	LWM, 10
$w(r_m, \frac{\pi}{6})$	2	1.436	1.43574	1.43576	1.43579	1.43592
	4	0.457	0.458150	0.458152	0.458155	0.458168
	10	0.144	0.143993	0.143993	0.143994	0.143994
$-\sigma_1(r_0, \frac{\pi}{6})$	2	0.0347	0.0346692	0.0346730	0.0346778	0.0347026
	4	0.0177	0.0177140	0.0177144	0.0177149	0.0177176
	10	0.0100	0.00994881	0.00994885	0.00994890	0.00994916
$\sigma_1(r_N, \frac{\pi}{6})$	2	0.0871	0.0871310	0.0871302	0.0871292	0.0871240
	4	0.0293	0.0292954	0.0292953	0.0292951	0.0292942
	10	0.0115	0.0114721	0.0114721	0.0114720	0.0114719
$-\sigma_2(r_0, \frac{\pi}{6})$	2	3.467	3.46692	3.46730	3.46778	3.47026
	4	1.772	1.77140	1.77144	1.77149	1.77176
	10	0.995	0.994881	0.994885	0.994890	0.994916
$\sigma_2(r_N, \frac{\pi}{6})$	2	2.463	2.46310	2.46302	2.46292	2.46240
	4	1.367	1.36704	1.36703	1.36701	1.36692
	10	0.897	0.897209	0.897207	0.897204	0.897190
$\sigma_3(r_m, 0)$	2	0.394	0.393518	0.393523	0.393528	0.393556
	4	0.476	0.475725	0.475727	0.475728	0.475736
	10	0.525	0.525113	0.525113	0.525114	0.525115

[a] LWM, l denotes that each separate layer in the laminated panel is divided into l sub-layers when LWM is employed.

analysis based on LWM can give a result of arbitrary precision, because when the number of sub-layers increases, the approximate laminate model will be more and more close to the original laminated structure. In the following calculations, when LWM is employed, we always assume that each layer in the laminated cylindrical panel is divided into 30 equal sub-layers, for which the results are highly accurate as shown in Table 1.

As mentioned in the last section, when the cylindrical panel is long enough along the z-axis, it can be seen as in a state of cylindrical bending for which $u_z = 0$ and all physical variables are independent of z. Table 2 gives the results of a three-ply perfect laminated cylindrical panel with different length-to-thickness ratios.

Comparing Table 2 with Table 1, one can see that when L/h increases, the results converge constantly to those for cylindrical bending. It is noted that for deflection calculation, a panel can be taken as being in a state of cylindrical bending even when L/h is as small as $4S$. The relative error of this handling, when compared to the exact solution in Table 1, is smaller than 4%. This conclusion is consistent with that obtained for a laminated rectangular plate by Whitney (1987). However, the stress component σ_z for $L/h = 4S$, especially at the top surface, is quite different from that given by the exact cylindrical bending. Thus, in practice, the assumption of cylindrical bending should be carefully used for the calculation of stresses. We also note that the deflection of the panel obtained under the assumption of cylindrical bending is the upper limit, which results from the fact that in the state of cylindrical bending, the constraints at the two edges $z = 0, L$ are released, i.e. the rigidity of the panel is reduced.

Table 3 compares the results of our method with those of the extended third-order zigzag shell theory (Cheng et al., 2000) for a three-ply ([90/0/90°]) laminated cylindrical panel subjected to sinusoidal load $p = -p_0 \sin(\pi\eta)(\sin \pi\zeta)$ at the bottom surface. It is assumed that the two interfaces are identical, i.e. $\bar{R}^{(1)} = \bar{R}^{(2)} = R$. For the sake of comparison, the following non-dimensional quantities (Cheng et al., 2000) are employed in Table 3:

Table 2
Validation of cylindrical bending assumption for a three-ply ([90/0/90°]) perfect cylindrical panel subjected to sinusoidal load $q = q_0 \sin(\pi\eta)\sin(\pi\zeta)$ at the top surface ($\alpha = \pi/3$)

Quantity	S	L/h			
		$4S$	$10S$	$100S$	$1000S$
$w(r_m, \frac{\pi}{6}, \frac{L}{2})$	2	1.38497	1.42977	1.43571	1.43576
	4	0.446222	0.457079	0.458145	0.458152
	10	0.139359	0.143704	0.143993	0.143993
$-\sigma_1(r_0, \frac{\pi}{6}, \frac{L}{2})$	2	0.0233162	0.0366425	0.0346897	0.0346732
	4	0.0177140	0.0179436	0.0177137	0.0177144
	10	0.00931996	0.00925565	0.00993941	0.00994875
$\sigma_1(r_N, \frac{\pi}{6}, \frac{L}{2})$	2	0.128345	0.0952157	0.0872165	0.0871310
	4	0.0471911	0.0330501	0.0293363	0.0292957
	10	0.0198365	0.0135056	0.0114952	0.0114723
$-\sigma_2(r_0, \frac{\pi}{6}, \frac{L}{2})$	2	3.32435	3.45058	3.46716	3.46730
	4	1.71884	1.76674	1.77141	1.77144
	10	0.958932	0.992630	0.994878	0.994885
$\sigma_2(r_N, \frac{\pi}{6}, \frac{L}{2})$	2	2.37537	2.45033	2.46290	2.46302
	4	1.32896	1.36238	1.36699	1.36703
	10	0.869806	0.894958	0.897194	0.897207
$\sigma_3(r_m, 0, 0)$	2	0.385510	0.392064	0.393510	0.393523
	4	0.464429	0.474693	0.475720	0.475727
	10	0.509392	0.524162	0.525111	0.525113

$$w' = \frac{10E_L}{p_0 h S^4} u_r, \quad \sigma_1' = \frac{10}{p_0 S^2}\sigma_z, \quad \sigma_2' = \frac{10}{p_0 S^2}\sigma_\theta, \quad \sigma_3' = \frac{10}{p_0 S}\tau_{r\theta}. \tag{25}$$

It is seen from Table 3 that, as expected, the present 3D solution for the perfect laminated panel is almost identical to that obtained by Varadan and Bhaskar (1991), whose results are however not presented here for brevity. We also found that Cheng et al. (2000) made two mistakes when quoting Varadan and Bhaskar (1991)'s original data: (1) the values of the deflection should be those at the mediate surfaces, not the bottom surfaces as claimed in Table 1 of that paper; and (2) the central deflection w' and the transverse shear stress σ_3' at $r = r_m$ for $S = 4$ should be 4.009 and 2.349, respectively.

Table 3 clearly shows that although the shell theory can give very good predictions for the moderately-thick, perfectly-bonded laminates, its predicting error becomes much larger at the presence of weak interface. For example, when $S = 10$, the relative errors [1] of the central deflection predicted by shell theory are −1.6%, 12.6%, 26.8%, and 40.0% for $R = 0.0$, 0.3, 0.6, and 0.9, respectively. In fact, even when $S = 50$, the relative error still has a value of 6.3% for $R = 0.9$. Further, as shown in Table 3, since the shell theory usually underestimates the transverse shear stress $\tau_{r\theta}$, one may have difficulty in evaluating the interfacial shear strength. Thus, for a laminated panel with interfaces seriously weakened, the validity of shell theory should be carefully cross-examined with available 3D exact solutions.

The distributions of stresses and displacements along the thickness direction are given in Fig. 2 for a five-ply asymmetric laminated cylindrical panel with $S = 4$, $\alpha = \pi/3$ and $L/h = 4S$. The stacking sequence is

[1] Defined as: (shell-3D)/3D.

Table 3
Comparison for a three-ply ([90/0/90°]) cylindrical panel with weak interfaces subjected to sinusoidal load $p = -p_0 \sin(\pi\eta)(\sin \pi\zeta)$ at the bottom surface ($L/h = 4S$, $\alpha = \pi/4$)[a]

Quantity	S	$R = 0.0$	$R = 0.3$	$R = 0.6$	$R = 0.9$
$w'(r_m, \frac{\pi}{8}, \frac{L}{2})$	4	4.00897	4.56004	5.01155	5.37336
		(3.60671)	(4.54355)	(5.22412)	(5.68617)
	10	1.22329	1.38630	1.54034	1.68613
		(1.20335)	(1.56068)	(1.95346)	(2.36049)
	50	0.54953	0.55683	0.56411	0.57135
		(0.54862)	(0.56474)	(0.58443)	(0.60760)
	100	0.47154	0.47300	0.47445	0.47590
		(0.47110)	(0.47432)	(0.47827)	(0.48293)
$\sigma_1'(r_0, \frac{\pi}{8}, \frac{L}{2})$	4	−0.27009	−0.28207	−0.29131	−0.29858
		(−0.12923)	(−0.15659)	(−0.17584)	(−0.18821)
	10	−0.07910	−0.82867	−0.08639	−0.07248
		(−0.05632)	(−0.06436)	(−0.07327)	(−0.08248)
	50	−0.02245	−0.02234	−0.02222	−0.02211
		(−0.02167)	(−0.02139)	(−0.02106)	(−0.02067)
	100	0.00183	0.00193	0.00203	0.00213
		(0.00197)	(0.00220)	(0.00247)	(0.00280)
$\sigma_1'(r_N, \frac{\pi}{8}, \frac{L}{2})$	4	0.12702	0.14119	0.15235	0.16133
		(0.12126)	(0.14641)	(0.16369)	(0.17444)
	10	0.07392	0.08023	0.08618	0.09179
		(0.07231)	(0.08561)	(0.10028)	(0.11544)
	50	0.07124	0.07180	0.07235	0.07290
		(0.07097)	(0.07215)	(0.07360)	(0.07531)
	100	0.08384	0.08401	0.08417	0.08434
		(0.08370)	(0.08406)	(0.08450)	(0.08502)
$\sigma_2'(r_0, \frac{\pi}{8}, \frac{L}{2})$	4	−9.32297	−10.36933	−11.21592	−11.91532
		(−10.52806)	(−12.94523)	(−14.80410)	(−16.14023)
	10	−5.22390	−5.57376	−5.90440	−6.85332
		(−5.30760)	(−6.04312)	(−6.87232)	(−7.74757)
	50	−3.98646	−3.99998	−4.01345	−4.02687
		(−3.98701)	(−4.01326)	(−4.04618)	(−4.08560)
	100	−3.50650	−3.50812	−3.50974	−3.51135
		(−3.50626)	(−3.50900)	(−3.51255)	(−3.51690)
$\sigma_2'(r_N, \frac{\pi}{8}, \frac{L}{2})$	4	6.54448	7.27688	7.86913	8.35815
		(7.01022)	(8.51118)	(9.67634)	(10.52132)
	10	4.68271	4.97600	5.25316	5.51549
		(4.69967)	(5.30698)	(5.99277)	(6.71749)
	50	3.93012	3.94335	3.95653	3.96966
		(3.92646)	(3.95217)	(3.98441)	(4.02301)
	100	3.50674	3.50841	3.51008	3.51175
		(3.50478)	(3.50766)	(3.51137)	(3.51592)
$\sigma_3'(r_m, 0, 0)$	4	2.34883	2.13149	1.96304	1.81160
		(2.00375)	(1.49511)	(1.09511)	(0.80258)
	10	3.26357	3.17793	3.09703	3.02049
		(3.24028)	(3.06610)	(2.86781)	(2.65714)
	50	3.49102	3.48478	3.47856	3.47236
		(3.48937)	(3.47683)	(3.46121)	(3.44259)
	100	3.12660	3.12398	3.12136	3.11874
		(3.12561)	(3.12009)	(3.11325)	(3.10511)

[a] Data in parentheses were obtained by Cheng et al. (2000).

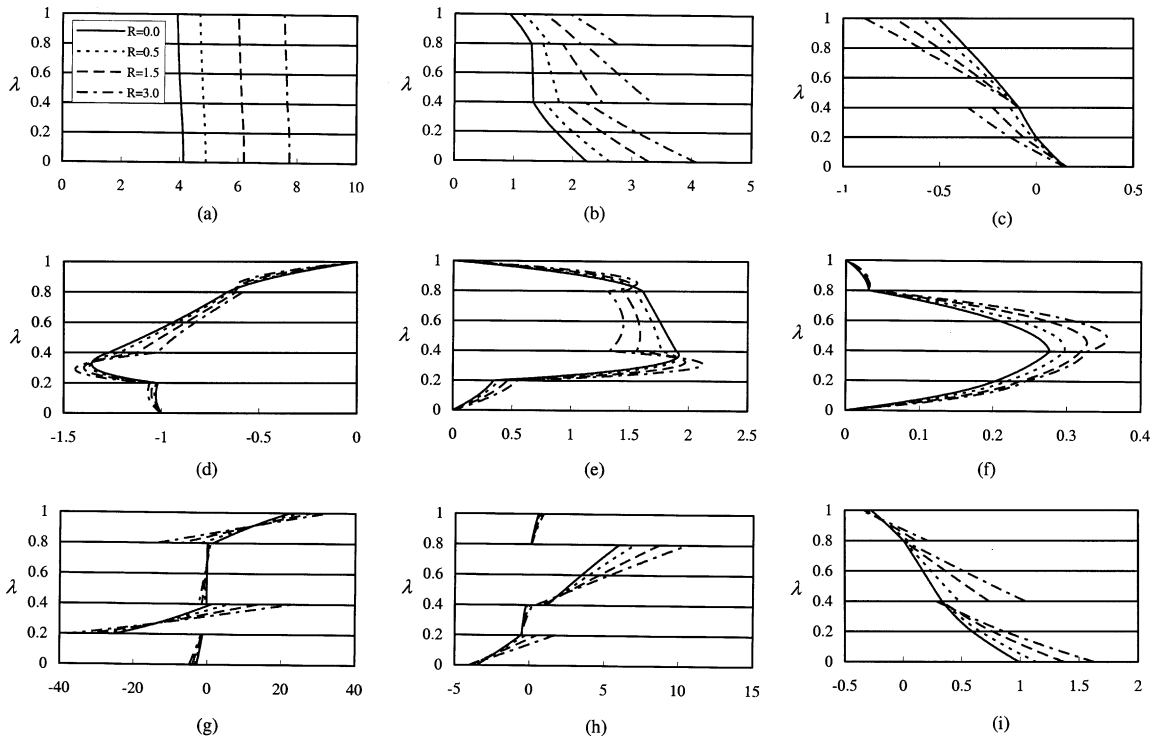

Fig. 2. Distributions of normalized physical variables along the thickness direction: (a) $u_r(r,\alpha/2,L/2)E_T/(p_0r_0)$, (b) $u_\theta(r,0,L/2)E_T/(p_0r_0)$, (c) $u_z(r,\alpha/2,0)E_T/(p_0r_0)$, (d) $\sigma_r(r,\alpha/2,L/2)/p_0$, (e) $\tau_{r\theta}(r,0,L/2)/p_0$, (f) $\tau_{rz}(r,\alpha/2,0)/p_0$, (g) $\sigma_\theta(r,\alpha/2,L/2)/p_0$, (h) $\sigma_z(r,\alpha/2,L/2)/p_0$, (i) $\tau_{\theta z}(r,0,0)/p_0$.

[90/0/0/90/0°] and the load is the same as that considered in Table 3. It is assumed that the first and third interfaces are perfect, while the second and fourth ones (from bottom) are weakened with $\bar{R}^{(2)} = 2\bar{R}^{(4)} = R$. For clarity purpose, a non-dimensional radial coordinate $\lambda = (r - r_0)/(r_N - r_0)$ is introduced in Fig. 2 such that $\lambda = 0$ and $\lambda = 1$ correspond to the bottom and top surfaces, respectively.

It is clearly seen that the displacement u_θ is discontinuous across the second and fourth interfaces and the displacement u_z is discontinuous across the second interface, because of the weakness introduced locally there ($R \neq 0$). The discontinuity of u_z at the fourth interface is however, not obvious because the shear stress τ_{rz} at the fourth interface is much smaller than the one at the second interface in this example. In a generally perfect laminate, the three stress components, σ_θ, σ_z, and $\tau_{\theta z}$ usually have discontinuities at the interfaces, however, they are continuous across the third interface in the present example because the third layer and fourth layer are the same. We also notice that for a cross-ply laminated cylindrical panel, since c_{66} of a particular ply does not depend on the fiber orientation, $\tau_{\theta z}$ is continuous across all interfaces in a perfect laminated panel, as shown in Fig. 2(i). When weak interfaces are present, the continuity of $\tau_{\theta z}$ will depend on the two displacements u_θ and u_z, which can be seen from the constitutive relations, Eq. (2). By comparing Fig. 2(e) with Fig. 2(f), we find that the effect of weak interface is different on the shear stresses $\tau_{r\theta}$ and τ_{rz}. In fact, $\tau_{r\theta}$ at the weak interfaces decreases with R, while τ_{rz} increases. Thus, if we want to prevent the bonding shear failure using technique of weakening interfaces, exact evaluation should be made *a priori* to select a proper degree of weakness.

Now we consider the free vibration problem. The lowest non-dimensional frequency parameter $\bar{\omega} = \omega h(L/h)^2\sqrt{\rho/(E_L S)}$ is given in Table 4 for the three-ply laminated cylindrical panel that was

Table 4
The lowest dimensionless frequency $\overline{\omega}$ for a three-ply ([90/0/90°]) cylindrical panel with weak interfaces ($L/h = 5S$, $\alpha = \pi/3$)[a]

(m,n)	S	$R = 0.0$	$R = 0.3$	$R = 0.6$	$R = 0.9$
(1,1)	4	11.66616	10.87918	10.31621	9.89192
		(11.99395)	(10.46062)	(9.51144)	(8.90386)
	10	12.86607	12.24169	11.71792	11.27108
		(12.95592)	(11.66571)	(10.57431)	(9.67627)
	20	11.20476	10.98330	10.77682	10.58373
		(11.23782)	(10.76221)	(10.26312)	(9.76555)
	50	8.19762	8.17022	8.14319	8.11654
		(8.20638)	(8.14615)	(8.07443)	(7.99254)
(1,2)	4	12.04638	11.29643	10.74769	10.33412
		(12.38716)	(10.89474)	(9.97441)	(9.38532)
	10	13.46939	12.86727	12.36408	11.93629
		(13.56426)	(12.32296)	(11.28327)	(10.43676)
	20	12.37615	12.17310	11.98442	11.80854
		(12.41403)	(11.97924)	(11.52694)	(11.08049)
	50	11.49005	11.47005	11.45035	11.43094
		(11.50035)	(11.45682)	(11.40519)	(11.34654)
(2,1)	4	30.73004	29.10653	28.05967	27.32793
		(34.63088)	(32.53590)	(31.71714)	(31.43851)
	10	39.32893	36.58271	34.54921	32.97619
		(39.67459)	(34.31803)	(30.72844)	(28.27173)
	20	41.23324	39.18662	37.47011	36.00582
		(41.30724)	(37.13336)	(33.59432)	(30.67520)
	50	32.68723	32.22254	31.77956	31.35668
		(32.70070)	(31.69756)	(30.59182)	(29.43239)
(2,2)	4	30.85077	29.23539	28.19291	27.46339
		(34.73297)	(32.64673)	(31.82869)	(31.54784)
	10	39.43239	36.69138	34.66231	33.09303
		(39.78115)	(34.43379)	(30.85229)	(28.40182)
	20	41.35086	39.30621	37.59177	36.12960
		(41.42976)	(37.25946)	(33.72556)	(30.81249)
	50	32.90136	32.43843	31.99722	31.57611
		(32.91889)	(31.91951)	(30.81842)	(29.66449)

[a] Data in parentheses were obtained by Cheng et al. (2000).

considered in Table 3, but with $L/h = 5S$ and $\alpha = \pi/3$. Comparison is also made against results obtained by the extended third-order zigzag shell theory (Cheng et al., 2000).

Table 4 shows that the lowest frequency decreases with R, indicating that the weak interfaces result in reduction of rigidity of the panel. This is consistent with the results of the bending problem in which the deflection increases with R under same surface pressure level (Table 3). Again, although the shell theory in Cheng et al. (2000) behaves well for the moderately thick shell, its accuracy degrades as R increases. For example, the relative errors with respect to the current 3D solution are 0.70%, −4.71%, −9.76%, and −14.15%, for $R = 0.0$, 0.3, 0.6 and 0.9, respectively when $S = 10$ and $m = n = 1$. It is also interesting to note that while the shell theory often tends to overestimate the lowest natural frequency of a perfect panel, it more often than less underestimates the frequency of a laminated panel with weak interfaces. Results shown in Table 4 are for $R = 0.3$, 0.6 and 0.9, and the shell theory always gives an underestimated frequency except for $S = 4$ and $(m,n) = (2,1)$ or $(m,n) = (2,2)$.

Table 5
Lowest natural frequency parameter ω^* of laminated cylindrical panels with weak interfaces ($S = 4$, $\alpha = \pi/3$, $m = n = 1$)

Stacking sequence	L/h	$R = 0$	$R = 0.3$	$R = 0.6$	$R = 0.9$
[0/90°]	$3S$	0.894755	0.886667	0.879385	0.872795
	$5S$	0.853011	0.845546	0.838840	0.832784
	$10S$	0.838351	0.831164	0.824712	0.818889
	$100S$	0.834976	0.827911	0.821568	0.815843
	$500S$	0.834952	0.827888	0.821546	0.815822
	∞	0.834951	0.827887	0.821545	0.815822
[0/90/0°]	$3S$	0.668142	0.656171	0.645833	0.636776
	$5S$	0.591202	0.584350	0.578095	0.572360
	$10S$	0.565970	0.560281	0.555027	0.550160
	$100S$	0.560931	0.555457	0.550395	0.545700
	$500S$	0.560899	0.555427	0.550367	0.545673
	∞	0.560898	0.555426	0.550365	0.545672
[0/90/0/90°]	$3S$	0.924195	0.850244	0.799007	0.761037
	$5S$	0.882528	0.808350	0.757251	0.719595
	$10S$	0.869644	0.795057	0.743728	0.705954
	$100S$	0.867454	0.792751	0.741349	0.703531
	$500S$	0.867444	0.792740	0.741337	0.703519
	∞	0.867444	0.792739	0.741337	0.703519
[$(0/90)_2$0°]	$3S$	0.791885	0.723517	0.676358	0.641449
	$5S$	0.733878	0.667181	0.621635	0.588183
	$10S$	0.716674	0.649706	0.604083	0.570662
	$100S$	0.713829	0.646741	0.601050	0.567595
	$500S$	0.713816	0.646727	0.601035	0.567580
	∞	0.713815	0.646726	0.601035	0.567580

The cylindrical bending assumption for free vibration problem is investigated in Table 5, where the lowest natural frequency parameter $\omega^* = \omega r_0\sqrt{\rho/E_T}$ for $m = n = 1$ is given. The formulations for cylindrical bending problem, e.g. Eq. (21) are directly employed to calculate the results for $L/h \to \infty$. All interfaces in the laminated cylindrical panel are assumed identical, i.e. $R = \bar{R}^{(1)} = \bar{R}^{(2)} = \cdots = \bar{R}^{(N-1)}$. It can be seen that the lowest frequency of the cylindrical panel converges rapidly to that of the panel in cylindrical bending when L/h increases. Also important to note that the accuracy of the results based on the cylindrical bending assumption is affected by the stacking sequence. This can be seen from the case of $L/h = 5S$, where the relative error of the frequency, when compared to that of cylindrical bending, is around 5% for the layup [0/90/0°]; while it is only about 2% for the layup [0/90°]. In contrast to the static problem, the frequency of the laminate in cylindrical bending is the lower limit, again resulting from constraint-free condition at $z = 0, L$.

Table 6 gives the first 10 lowest non-dimensional natural frequencies ($\omega^* = \omega r_0\sqrt{\rho/E_T}$) of the laminated cylindrical panel that was considered in Fig. 2 for three groups of (m, n). It can be shown that the effect of weak interfaces on the frequencies is quite different for different frequency order. For example, when $m = n = 1$, the relative error of the lowest frequency for $R = 0.9$ is up to 13.62% (compared to $R = 0.0$), while that of the second frequency is only 0.51%. In practice, if engineers want to know if the interfaces of a laminated structure are weakened or how much the degree of weakness of interfaces is by using non-destructive dynamic technology, this observation should be very important. In fact, one should select the mode, whose frequency is most sensitive to the weakness of interfaces, to perform the evaluation of practical structures.

Table 6
Lowest 10 frequency parameters ω^* of a five-ply ([90/0/0/90/0°]) laminated cylindrical panel with weak interfaces ($S = 4$, $\alpha = \pi/3$ and $L/h = 4S$)

(m,n)	Order	$R = 0.0$	$R = 0.3$	$R = 0.6$	$R = 0.9$
(1,1)	1	0.82284	0.77708	0.74063	0.71079
	2	3.23737	3.23189	3.22634	3.22071
	3	7.13570	6.56476	6.12657	5.78278
	4	7.89221	7.46391	7.07489	6.73682
	5	9.16483	9.07649	9.02195	8.98411
	6	12.13538	11.51811	10.80907	10.17484
	7	12.52188	12.16021	11.96772	11.82246
	8	13.79163	13.44340	13.25300	13.14420
	9	18.61502	18.08920	17.30980	16.77760
	10	19.15239	18.12282	17.68995	17.27979
(2,1)	1	2.16713	2.04683	1.95961	1.89321
	2	4.54656	4.53942	4.53209	4.52459
	3	7.87119	7.35520	6.96643	6.66642
	4	9.95547	9.36789	8.84303	8.41987
	5	11.89417	11.50341	11.17338	10.61777
	6	12.74625	11.99839	11.43959	11.27952
	7	13.58080	13.34172	13.24994	13.20382
	8	19.15603	18.03080	17.21865	16.62966
	9	19.43145	18.39950	17.63478	17.11821
	10	23.27820	22.96347	22.72936	22.42300
(1,2)	1	0.95072	0.90453	0.86764	0.83739
	2	5.46950	5.41384	5.35589	5.29543
	3	7.91592	7.50076	7.12120	6.78898
	4	8.32288	7.76416	7.33994	7.01397
	5	9.23426	9.13590	9.07668	9.03635
	6	12.16421	11.91090	11.57153	11.14859
	7	13.33419	12.69939	12.24408	11.95084
	8	13.81273	13.46958	13.27938	13.16959
	9	18.63395	18.13145	17.68316	17.20243
	10	19.57440	18.52798	17.77046	17.31957

6. Conclusions

In this paper, state-space formulations are established to investigate the static and dynamic behaviors of simply-supported cross-ply laminated cylindrical panels with weak interfaces, which are modeled as general linear spring-layers. Compared to the previous work on perfect laminated cylindrical panels, the only additional element needs to be introduced is the interfacial transfer matrix, which can be easily integrated into the global transfer matrix. Numerical comparison shows that the present analysis based on the layer-wise model is of high accuracy compared to classic laminate theories. In fact, this method can give results of an arbitrary precision simply by increasing the number of sub-layers. It is also found that, while the extended zigzag shell theory developed by Cheng et al. (2000) does work well for perfect laminated panels, it becomes (much) less accurate for laminated cylindrical panel with weak interfaces, especially when the weakness is significant.

It is also emphasized here that although the shell theory gives conservative predictions of deflections and lowest natural frequencies ($m = n = 1$), as shown in Tables 3 and 4, respectively, the situation may become serious for the health diagnosis of structures in service. For example, if we obtain the central deflection (w') around 0.564 by experimental testing for $S = 50$, we may conclude that the panel has weak interfaces with

$R = 0.3$ by comparing with the shell theory's prediction (Table 3). However, from the 3D results, it actually corresponds to $R = 0.6$, which is more dangerous. To avoid this, highly accurate analysis methods are especially desired.

The cylindrical bending of the laminated panel is also considered in the paper. In particular, an exact state-space analysis is derived in Appendix B for the static loading case, which serves a benchmark to calibrate the LWM employed in the paper. Numerical investigation shows that the employment of assumption of cylindrical bending of a practical panel also should be careful.

Acknowledgements

The work was supported by the National Natural Science Foundation of China (No. 10002016). The first author also would like to express his sincere thanks to Dr. Q.D. Yang at Rockwell Scientific Company, California. The kind suggestions from the two anonymous reviewers are also acknowledged.

Appendix A. Matrices N(r) and A(ξ), and induced variables

The operator matrix $\mathbf{N}(r)$ is

$$\begin{aligned}
\mathbf{N}(r) &= \begin{bmatrix} \mathbf{N}_1(r) & \mathbf{N}_2(r) \\ \mathbf{N}_3(r) & \mathbf{N}_4(r) \end{bmatrix}, \\
\mathbf{N}_1(r) &= \begin{bmatrix} -\frac{c_{23}}{c_{33}}\frac{1}{r} & -\frac{c_{23}}{c_{33}}\frac{1}{r}\frac{\partial}{\partial\theta} & -\frac{c_{13}}{c_{33}}\frac{\partial}{\partial z} \\ -\frac{1}{r}\frac{\partial}{\partial\theta} & \frac{1}{r} & 0 \\ -\frac{\partial}{\partial z} & 0 & 0 \end{bmatrix}, \quad \mathbf{N}_2(r) = \begin{bmatrix} \frac{1}{c_{33}} & 0 & 0 \\ 0 & \frac{1}{c_{44}} & 0 \\ 0 & 0 & \frac{1}{c_{55}} \end{bmatrix}, \\
\mathbf{N}_3(r) &= \begin{bmatrix} \rho\frac{\partial^2}{\partial t^2} + \frac{k_3}{r^2} & \frac{k_3}{r^2}\frac{\partial}{\partial\theta} & \frac{k_2}{r}\frac{\partial}{\partial z} \\ -\frac{k_3}{r^2}\frac{\partial}{\partial\theta} & \rho\frac{\partial^2}{\partial t^2} - \frac{k_3}{r^2}\frac{\partial^2}{\partial\theta^2} - c_{66}\frac{\partial^2}{\partial z^2} & -\frac{c_{66}+k_2}{r}\frac{\partial^2}{\partial\theta\partial z} \\ -\frac{k_2}{r}\frac{\partial}{\partial z} & -\frac{c_{66}+k_2}{r}\frac{\partial^2}{\partial\theta\partial z} & \rho\frac{\partial^2}{\partial t^2} - \frac{c_{66}}{r^2}\frac{\partial^2}{\partial\theta^2} - k_1\frac{\partial^2}{\partial z^2} \end{bmatrix}, \\
\mathbf{N}_4(r) &= \begin{bmatrix} \left(\frac{c_{23}}{c_{33}} - 1\right)\frac{1}{r} & -\frac{1}{r}\frac{\partial}{\partial\theta} & -\frac{\partial}{\partial z} \\ -\frac{c_{23}}{c_{33}}\frac{1}{r}\frac{\partial}{\partial\theta} & -\frac{2}{r} & 0 \\ -\frac{c_{13}}{c_{33}}\frac{\partial}{\partial z} & 0 & -\frac{1}{r} \end{bmatrix},
\end{aligned} \tag{A.1}$$

where ρ is the mass density, and

$$k_1 = c_{11} - c_{13}^2/c_{33}, \quad k_2 = c_{12} - c_{13}c_{23}/c_{33}, \quad k_3 = c_{22} - c_{23}^2/c_{33}. \tag{A.2}$$

The three induced variables can be determined from the state variables by

$$\begin{aligned}
\sigma_z &= k_1\frac{\partial u_z}{\partial z} + k_2\left(\frac{1}{r}\frac{\partial u_\theta}{\partial\theta} + \frac{u_r}{r}\right) + \frac{c_{13}}{c_{33}}\sigma_r, \\
\sigma_\theta &= k_2\frac{\partial u_z}{\partial z} + k_3\left(\frac{1}{r}\frac{\partial u_\theta}{\partial\theta} + \frac{u_r}{r}\right) + \frac{c_{23}}{c_{33}}\sigma_r, \\
\tau_{\theta z} &= c_{66}\left(\frac{\partial u_\theta}{\partial z} + \frac{1}{r}\frac{\partial u_z}{\partial\theta}\right).
\end{aligned} \tag{A.3}$$

The non-dimensional coefficient matrix $\mathbf{A}(\xi)$ is

$$\mathbf{A}(\xi)=\begin{bmatrix}\mathbf{A}_1(\xi) & \mathbf{A}_2(\xi)\\ \mathbf{A}_3(\xi) & \mathbf{A}_4(\xi)\end{bmatrix},$$

$$\mathbf{A}_1(\xi)=\begin{bmatrix}-\frac{c_{23}}{c_{33}}\frac{1}{\xi} & \frac{c_{23}}{c_{33}}\frac{t_\alpha}{\xi} & \frac{c_{13}}{c_{33}}t_{\mathrm{L}}\\ -\frac{t_\alpha}{\xi} & \frac{1}{\xi} & 0\\ -t_{\mathrm{L}} & 0 & 0\end{bmatrix},\quad \mathbf{A}_2(\xi)=\begin{bmatrix}\frac{c_{44}^{(1)}}{c_{33}} & 0 & 0\\ 0 & \frac{c_{44}^{(1)}}{c_{44}} & 0\\ 0 & 0 & \frac{c_{44}^{(1)}}{c_{55}}\end{bmatrix},$$

$$\mathbf{A}_3(\xi)=\begin{bmatrix}-\frac{\rho}{\rho^{(1)}}\Omega^2+\frac{k_3}{c_{44}^{(1)}}\frac{1}{\xi^2} & -\frac{k_3}{c_{44}^{(1)}}\frac{t_\alpha}{\xi^2} & -\frac{k_2}{c_{44}^{(1)}}\frac{t_{\mathrm{L}}}{\xi}\\ -\frac{k_3}{c_{44}^{(1)}}\frac{t_\alpha}{\xi^2} & -\frac{\rho}{\rho^{(1)}}\Omega^2+\frac{k_3}{c_{44}^{(1)}}\frac{t_\alpha^2}{\xi^2}+\frac{c_{66}}{c_{44}^{(1)}}t_{\mathrm{L}}^2 & \frac{c_{66}+k_2}{c_{44}^{(1)}}\frac{t_\alpha t_{\mathrm{L}}}{\xi}\\ -\frac{k_2}{c_{44}^{(1)}}\frac{t_{\mathrm{L}}}{\xi} & \frac{c_{66}+k_2}{c_{44}^{(1)}}\frac{t_\alpha t_{\mathrm{L}}}{\xi} & -\frac{\rho}{\rho^{(1)}}\Omega^2+\frac{c_{66}}{c_{44}^{(1)}}\frac{t_\alpha^2}{\xi^2}+\frac{k_1}{c_{44}^{(1)}}t_{\mathrm{L}}^2\end{bmatrix},\tag{A.4}$$

$$\mathbf{A}_4(\xi)=\begin{bmatrix}\left(\frac{c_{23}}{c_{33}}-1\right)\frac{1}{\xi} & \frac{t_\alpha}{\xi} & t_{\mathrm{L}}\\ -\frac{c_{23}}{c_{33}}\frac{t_\alpha}{\xi} & -\frac{2}{\xi} & 0\\ -\frac{c_{13}}{c_{33}}t_{\mathrm{L}} & 0 & -\frac{1}{\xi}\end{bmatrix},$$

where $t_\alpha=m\pi/\alpha$, $t_{\mathrm{L}}=n\pi r_0/L$, and $\Omega=\omega r_0\sqrt{\rho^{(1)}/c_{44}^{(1)}}$ is the non-dimensional frequency.

Appendix B. Exact static analysis of cross-ply laminated cylindrical panel in cylindrical bending

For the static problem, Eq. (21) can be rewritten as

$$r\frac{\partial}{\partial r}\begin{Bmatrix}u_\theta\\ u_r\\ r\tau_{r\theta}\\ r\sigma_r\end{Bmatrix}=\begin{bmatrix}1 & -\frac{\partial}{\partial\theta} & \frac{1}{c_{44}} & 0\\ -\frac{c_{23}}{c_{33}}\frac{\partial}{\partial\theta} & -\frac{c_{23}}{c_{33}} & 0 & \frac{1}{c_{33}}\\ -k_3\frac{\partial^2}{\partial\theta^2} & -k_3\frac{\partial}{\partial\theta} & -1 & -\frac{c_{23}}{c_{33}}\frac{\partial}{\partial\theta}\\ k_3\frac{\partial}{\partial\theta} & k_3 & -\frac{\partial}{\partial\theta} & \frac{c_{23}}{c_{33}}\end{bmatrix}\begin{Bmatrix}u_\theta\\ u_r\\ r\tau_{r\theta}\\ r\sigma_r\end{Bmatrix}.\tag{B.1}$$

After the following variable substitution (Chen and Ding, 2001)

$$r=r_{k-1}\exp(\xi)\quad(k=1,2,\ldots,N;\ 0\leqslant\xi\leqslant\chi_k),\tag{B.2}$$

where $\chi_k=\ln(r_k/r_{k-1})$, Eq. (B.1) becomes

$$\frac{\partial}{\partial\xi}\begin{Bmatrix}u_\theta\\ u_r\\ r\tau_{r\theta}\\ r\sigma_r\end{Bmatrix}=\begin{bmatrix}1 & -\frac{\partial}{\partial\theta} & \frac{1}{c_{44}} & 0\\ -\frac{c_{23}}{c_{33}}\frac{\partial}{\partial\theta} & -\frac{c_{23}}{c_{33}} & 0 & \frac{1}{c_{33}}\\ -k_3\frac{\partial^2}{\partial\theta^2} & -k_3\frac{\partial}{\partial\theta} & -1 & -\frac{c_{23}}{c_{33}}\frac{\partial}{\partial\theta}\\ k_3\frac{\partial}{\partial\theta} & k_3 & -\frac{\partial}{\partial\theta} & \frac{c_{23}}{c_{33}}\end{bmatrix}\begin{Bmatrix}u_\theta\\ u_r\\ r\tau_{r\theta}\\ r\sigma_r\end{Bmatrix}\quad(k=1,2,\ldots,N;\ 0\leqslant\xi\leqslant\chi_k).\tag{B.3}$$

If we take a solution in a similar form of Eq. (5), except that the variation with z is disregarded owing to infinity condition along this dimension, the simply-supported condition at $\theta=0,\alpha$ (Ren, 1987) is then automatically satisfied. We then can derive a state equation with constant coefficients, of which the exact solution can be easily written out. The reader is referred to Chen and Ding (2001) for the detailed procedure.

References

Aboudi, J., 1987. Damage in composites-modelling of imperfect bonding. Composites Science and Technology 28, 103–128.

Bahar, L.Y., 1975. A state space approach to elasticity. Journal of the Franklin Institute 299, 33–41.

Barbero, E.J., Reddy, J.N., 1991. Modeling of delamination in composite laminates using a layer-wise plate theory. International Journal of Solids and Structures 28, 373–388.

Barbero, E.J., Luciano, R., Sacco, E., 1995. Three-dimensional plate and contact/friction elements for laminated composite joints. Computers & Structures 54, 689–703.

Bellman, R., 1970. Introduction to Matrix Analysis. McGraw-Hill, New York.

Chaboche, J.L., Feyel, F., Monerie, Y., 2001. Interface debonding models: a viscous regularization with a limited rate dependency. International Journal of Solids and Structures 38, 3127–3160.

Chen, W.Q., Ding, H.J., 2001. A state-space-based stress analysis of a multi-layered spherical shell with spherical isotropy. Journal of Applied Mechanics 68, 109–114.

Chen, W.Q., Cai, J.B., Ye, G.R., 2003. Exact solutions of cross-ply laminates with bonding imperfections. AIAA Journal 41, 2244–2250.

Cheng, Z.Q., Jemah, A.K., Williams, F.W., 1996a. Theory for multilayered anisotropic plates with weakened interfaces. Journal of Applied Mechanics 63, 1019–1026.

Cheng, Z.Q., Kennedy, D., Williams, F.W., 1996b. Effect of interfacial imperfection on buckling and bending behavior of composite laminates. AIAA Journal 34, 2590–2595.

Cheng, Z.Q., He, L.H., Kitipornchai, S., 2000. Influence of imperfect interfaces on bending and vibration of laminated composite shells. International Journal of Solids and Structures 37, 2127–2150.

Clegg, W.J., 1992. The fabrication and failure of laminar ceramic composites. Acta Metallurgica et Materialia 40, 3085–3093.

Di Sciuva, M., 1997. Geometrically nonlinear theory of multilayered plates with interlayer slips. AIAA Journal 35, 1753–1759.

Fan, J.R., Ye, J.Q., 1990. An exact solution for the statics and dynamics of laminated thick plates with orthotropic layer. International Journal of Solids and Structures 26, 655–662.

Fan, J.R., Zhang, J.Y., 1992a. Exact solutions for thick laminated shells. Science in China A 35, 1343–1355.

Fan, J.R., Zhang, J.Y., 1992b. Analytical solutions for thick, doubly curved, laminated shells. Journal of Engineering Mechanics 118, 1338–1356.

Hashin, Z., 1990. Thermoelastic properties of fiber composites with imperfect interface. Mechanics of Materials 8, 333–348.

Hashin, Z., 1991. Thermoelastic properties of particulate composites with imperfect interface. Journal of the Physics and Mechanics of Solids 39, 745–762.

Jing, H.S., Tzeng, K.G., 1995. Elasticity solution for laminated anisotropic cylindrical panels in cylindrical bending. Composite Structures 30, 307–317.

Jones, R.M., 1975. Mechanics of Composite Materials. Hemisphere, New York.

Khdeir, A.A., Reddy, J.N., 1997. An exact solution for the bending of thin and thick cross-ply laminated beams. Composite Structures 37, 195–203.

Kuo, D.H., Kriven, W.M., 1996. Chemical stability, microstructure and mechanical behavior of $LaPO_4$-containing ceramics. Materials Science and Engineering A 210, 123–134.

Librescu, L., Schmidt, R., 2001. A general linear theory of laminated composite shells featuring interlaminar bonding imperfections. International Journal of Solids and Structures 38, 3355–3375.

Liu, D., Xu, L., Lu, X., 1994. Stress analysis of imperfect composite laminates with an interlaminar bonding theory. International Journal for Numerical Methods in Engineering 37, 2819–2839.

Noor, A.K., Burton, W.S., 1990. Assessment of computational models for multilayered composite shells. Applied Mechanics Reviews 43, 67–97.

Pagano, N.J., 1969. Exact solutions for composite laminates in cylindrical bending. Journal of Composite Materials 3, 398–411.

Point, N., Sacco, E., 1995. A delamination model for laminated composites. International Journal of Solids and Structures 33, 483–509.

Ren, J.G., 1987. Exact solutions for laminated cylindrical shells in cylindrical bending. Composite Science and Technology 29, 169–187.

Soldatos, K.P., Shu, X.P., 2001. Modelling of perfectly and weakly bonded laminated plates and shallow shells. Composite Science and Technology 61, 247–260.

Srinivas, S., Rao, A.K., 1970. Bending, vibration and buckling of simply supported thick orthotropic rectangular plates and laminates. International Journal of Solids and Structures 6, 1463–1481.

Tarn, J.Q., 2002. A state space formalism for anisotropic elasticity. Part II: Cylindrical anisotropy. International Journal of Solids and Structures 39, 5157–5172.

Tenek, L.H., Henneke II, E.G., Gunzburger, M.D., 1993. Vibration of delaminated composite plates and some applications to non-destructive testing. Composite Structures 23, 253–262.

Varadan, T.K., Bhaskar, K., 1991. Bending of laminated orthotropic cylindrical shells—An elasticity approach. Composite Structures 17, 141–156.

Vlasov, V.Z., Leontev, N.N., 1966. Beams, Plates and Shells on Elastic Foundations. TTF-357, TT65-50135, NASA.

Whitney, J.M., 1987. Structural Analysis of Laminated Anisotropic Plates. Technomic Publishing Company, Lancaster.

Williams, T.O., Addessio, F.L., 1997. A general theory for laminate plates with delaminations. International Journal of Solids and Structures 34, 2003–2024.

Xu, K.M., Noor, A.K., 1996. Three-dimensional analytical solutions for coupled thermoelectroelastic response of multi-layered cylindrical shells. AIAA Journal 34, 802–812.

Ye, J.Q., Soldatos, K.P., 1994. Three-dimensional stress analysis of orthotropic and cross-ply laminated hollow cylinders and cylindrical panels. Computer Methods in Applied Mechanics and Engineering 117, 331–351.

Zeng, Y.P., Jiang, D.L., 2001. Fabrication and properties of laminated Al_2O_3/TiC composites. Ceramics International 27, 597–602.